Inorganic Chemistry

Article

pubs.acs.org/IC

Perovskite-to-Postperovskite Transitions in $NaNiF_3$ and $NaCoF_3$ and Disproportionation of $NaCoF_3$ Postperovskite under High Pressure and High Temperature

Hitoshi Yusa,*[,†] Yuichi Shirako,[‡] Masaki Akaogi,[‡] Hiroshi Kojitani,[‡] Naohisa Hirao,[§] Yasuo Ohishi,[§] and Takumi Kikegawa[⊥]

[†]National Institute for Materials Science, 1-1 Namiki, Tsukuba 305-0044, Japan

[‡]Department of Chemistry, Gakushuin University, 1-5-1 Mejiro, Toshima-ku, Tokyo 171-8588, Japan

[§]Japan Synchrotron Radiation Research Institute (JASRI), 1-1-1 Kouto, Sayo-cho 679-5198, Japan

[⊥]Institute of Materials Structure Science, High Energy Accelerator Research Organization (KEK), 1-1 Oho, Tsukuba 305-0801, Japan

ABSTRACT: High-pressure structural phase transitions in $NaNiF_3$ and $NaCoF_3$ were investigated by conducting in situ synchrotron powder X-ray diffraction experiments using a diamond anvil cell. The perovskite phases ($GdFeO_3$ type) started to transform into postperovskite phases ($CaIrO_3$ type) at about 11−14 GPa, even at room temperature. The transition pressure is much lower than those of oxide perovskites. The anisotropic compression behavior led to heavily tilted octahedra that triggered the transition. Unlike oxide postperovskites, fluoropostperovskites remained after decompression to 1 atm. The postperovskite phase in $NaCoF_3$ broke down into a mixture of unknown phases after laser heating above 26 GPa, and the phases changed into amorphous ones when the pressure was released. High-pressure and high-temperature experiments using a multianvil apparatus were also conducted to elucidate the phase relations in $NaCoF_3$. Elemental analysis of the recovered amorphous samples indicated that the $NaCoF_3$ postperovskite disproportionated into two phases. This kind of disproportionation was not evident in $NaNiF_3$ even after laser heating at 54 GPa. In contrast to the single postpostperovskite phase reported in $NaMgF_3$, such a postpostperovskite phase was not found in the present compounds.

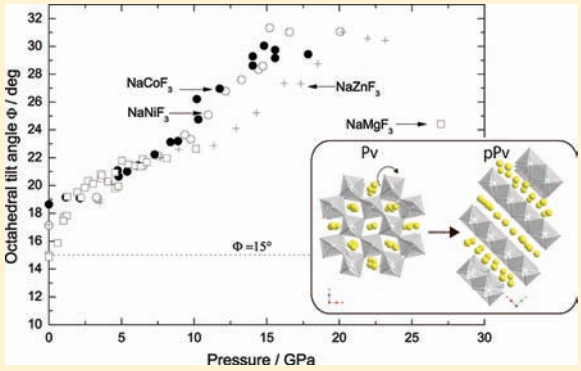

INTRODUCTION

Since the postperovskite structure (space group: *Cmcm*) was discovered in $MgSiO_3$,[1] high-pressure phase transitions in many silicates, germanates, titanates, and stannates, representing $A^{2+}B^{4+}O_3$ orthorhombic perovskites (space group: *Pnma*), have been reexamined to see whether they have this phase as well.[2−7] Some germanates ($MgGeO_3$ and $MnGeO_3$)[2,3] and a stannate ($CaSnO_3$)[4] have been found to crystallize into the $CaIrO_3$-type postperovskite structure, whereas other germanates (e.g., $CaGeO_3$ and $CdGeO_3$) and stannates (e.g., $CdSnO_3$ and $MnSnO_3$) have yet to be shown to have this kind of phase. Moreover, titanate perovskites decompose into mixtures of two phases, as has recently been shown in $FeTiO_3$ and $MnTiO_3$.[5−7]

Compared with the extensive research on postperovskite phases in oxide perovskites, research on fluoroperovskites ($A^+B^{2+}F_3$) has been rather limited. In particular, postperovskites have not been found yet in $KB^{2+}F_3$ (B = Mg, Zn, Ni, Co), which are cubic perovskite structures under ambient conditions.[8] To date, in situ X-ray diffraction (XRD) experiments have confirmed that $NaMgF_3$ (neighborite) and $NaZnF_3$ perovskites, which are isostructural to $MgSiO_3$ perovskite, have postperovskite phases.[9−11] Compared with the oxide postperovskites mentioned above, these fluoropostperovskites crystallized at room temperature and relatively low pressure, i.e., 30 GPa for $NaMgF_3$ and 18 GPa for $NaZnF_3$.

A further transformation to a postpostperovskite in $NaMgF_3$ was suggested by Martin et al.,[9] although the existence of this phase is still controversial.[12] They proposed a possible structure (space group: *Pnnm*), an N phase as the authors called it, for the diffraction profile from the laser-heated sample above 35 GPa. Yakovlev et al.[11] reported that an additional peak appeared on the diffraction profile in the $NaZnF_3$ postperovskite above 25 GPa, even when the compression was conducted at room temperature. Thus, the study of fluoroperovskites under high pressure should be significant not only for checking whether they have perovskite-to-postperovskite transitions but also for finding the key to understanding postpostperovskite transitions.

In this study, we treated other sodium fluoroperovskites with the $NaB^{2+}F_3$ (B = Ni, Co) composition. Considering that B^{2+} has a cationic radius similar to those of Mg^{2+} and Zn^{2+}, we speculated that these orthorhombic perovskites would transform into postperovskites. Lately, in fact, a bulk $NaNiF_3$

Received: January 17, 2012
Published: June 1, 2012

 © 2012 American Chemical Society dx.doi.org/10.1021/ic300118d | *Inorg. Chem.* 2012, 51, 6559−6566

postperovskite phase was successfully synthesized from fluoride mixtures by using a multianvil high-pressure apparatus at 15−18 GPa and 1200−1500 K.[13] Here, we report on the high-pressure behavior of $NaB^{2+}F_3$ (B = Ni, Co), as examined in in situ synchrotron radiation XRD (SXRD) experiments using a diamond anvil cell (DAC). In addition to room-temperature compression experiments, laser-heating experiments were conducted to accelerate the phase transition. Particularly, higher pressure was applied in the laser-heating experiments in order to explore the possibility of postpostperovskite transitions. In an attempt to draw a precise phase diagram, we also tried to synthesize $NaCoF_3$ perovskite and postperovskite by using a multianvil high-pressure apparatus. On the basis of the present results, we were able to reveal the peculiar character of sodium fluoroperovskites in comparison with oxide perovskites.

EXPERIMENTAL SECTION

The samples for the in situ SXRD experiments were prepared by using the multianvil high-pressure apparatus. For the $NaNiF_3$ perovskite synthesis, an equimolar mixture of NaF and NiF_2 packed into a gold capsule was put in a boron nitride sleeve. The sleeve was inserted in a cylindrical platinum heater, and the heater was placed in the pressure medium of a semisintered MgO octahedron. The temperature was measured by a Pt−Pt/13% Rh thermocouple positioned in the central part of the platinum heater. The sample was compressed to 12 GPa and heated at 1273 K for 30 min. Another $NaCoF_3$ perovskite sample was synthesized by keeping an equimolar mixture of NaF and CoF_2 at 15 GPa and 1273 K for 30 min by means of the same method as that used in the $NaNiF_3$ perovskite synthesis. Each recovered product was confirmed by XRD to be a single phase of $NaNiF_3$ or $NaCoF_3$ perovskite. The lattice parameters of the synthesized perovskites are consistent with those in the literature.[14]

Each sample was crushed in a corundum mortar and mixed with a small amount of gold powder (~0.1 wt %) as a pressure scale. A symmetric DAC (Syntek Co., Ltd.) was used for the in situ high-pressure experiments. The samples were loaded into 100−150-μm-diameter holes in a 60−80-μm-thick rhenium gasket filled with a hydrostatic medium (methanol:ethanol:water = 16:3:1). A pressure medium was not used in the laser-heating experiments in order to avoid unexpected reactions at high temperature. The in situ SXRD experiments at room temperature were conducted at BL04B2 (SPring-8, JASRI) and AR-NE1 (Photon Factory, KEK) using 38 and 30 keV monochromatic X-rays, respectively. The incident X-rays were collimated to ~50 μm and focused on the sample in the DAC. The diffracted X-rays were detected with an imaging plate (IP), typically for 10 min. The Debye rings recorded on the IP were converted into intensity versus 2θ data by using the *FIT2D* program.[15] The laser-heating experiments were carried out at BL10XU (SPring-8, JASRI). These experiments used a double-sided Nd:YAG laser beam focused to a 30-μm-diameter spot on the sample. The temperature was monitored by measuring the gray-body radiation emitted from the sample. The laser beam scanned all parts of the sample at a step interval of 10 μm. A charge-coupled device (CCD) was also used to detect the diffracted X-rays. The combination of the powerful X-ray source at BL10XU and the CCD detector enabled us to perform a quick X-ray exposure during laser heating. However, we could not observe any high-temperature phase during laser heating under high pressure. Therefore, we mainly collected the XRD data after laser heating.

Because of the complexity of the phase relations of $NaCoF_3$ polymorphs, we repeatedly conducted recovery experiments by using the multianvil high-pressure apparatus over a wide $P-T$ range, i.e., 14−23.4 GPa and 1173−1473 K. Details of these high-pressure and high-temperature experiments were the same as those described in the previous paper.[13] The recovered samples were characterized using a microfocus X-ray diffractometer (Rigaku RINT2500 V), a scanning electron microscope (JEOL JSM-6360), and an electron probe microanalyzer (JEOL JXA-8500F).

RESULTS AND DISCUSSION

Perovskite-to-Postperovskite Transition in $NaNiF_3$. The SXRD profiles from the $NaNiF_3$ sample under high pressure are indicated in Figure 1. The X-ray peak gradually

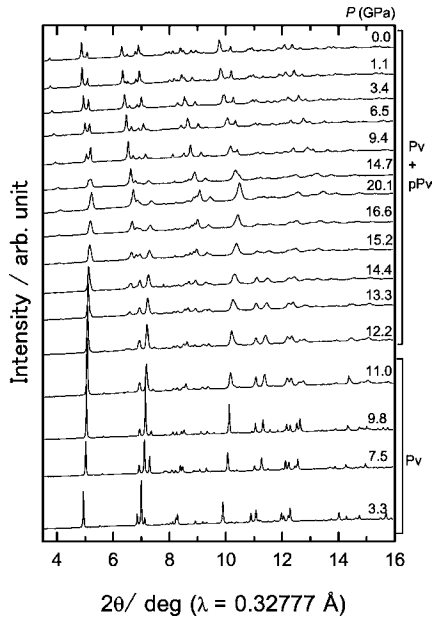

Figure 1. XRD profiles from the $NaNiF_3$ sample under room-temperature compression using a quasihydrostatic pressure medium. Pv and pPv denote the perovskite and postperovskite phases in the diffraction profile. The pressure changes from bottom to top.

broadened because of the increase in nonhydrostaticity in the pressure medium above 11 GPa. However, a profile fitting the Le Bail method (GSAS)[16] yielded a good enough resolution for a peak assignment to be made (Figure 2). All of the lattice

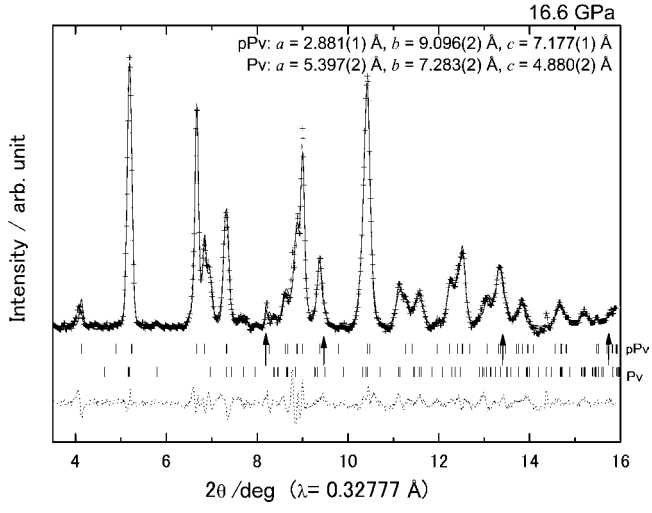

Figure 2. XRD profile with the Le Bail method (GSAS) for perovskite and postperovskite in $NaNiF_3$ at 16.6 GPa. Tick marks represent the calculated positions of the diffraction peaks of the perovskite (bottom) and postperovskite (top). Arrows indicate the positions of the diffractions from gold powder. R_{wp} = 1.0%.

dx.doi.org/10.1021/ic300118d | *Inorg. Chem.* 2012, 51, 6559−6566

parameters are shown in Table 1. The starting single perovskite phase was found to turn into a two-phase mixture of perovskite

Table 1. Unit Cell Parameters and Cell Volumes of $NaNiF_3$ Perovskites (Pv) and Postperovskites (pPv) under Quasihydrostatic Compression

P(GPa)	a (Å)	b (Å)	c (Å)	V (Å^3)	phase
3.3	5.483(0)	7.598(0)	5.275(0)	219.74(1)	Pv
7.5	5.429(0)	7.468(0)	5.153(0)	208.94(1)	Pv
9.8	5.417(0)	7.434(0)	5.113(0)	205.90(1)	Pv
11.0	5.417(0)	7.399(0)	5.065(1)	203.02(1)	Pv
	2.923(3)	9.394(9)	7.235(7)	198.66(21)	pPv
12.2	5.420(1)	7.378(1)	5.026(1)	201.01(2)	Pv
	2.895(4)	9.347(13)	7.236(7)	195.77(26)	pPv
13.3	5.416(1)	7.354(1)	4.996(1)	199.01(2)	Pv
	2.878(2)	9.292(6)	7.233(3)	193.44(11)	pPv
14.4	5.411(1)	7.329(1)	4.968(1)	197.04(3)	Pv
	2.886(1)	9.232(4)	7.214(2)	192.23(6)	pPv
15.2	5.414(3)	7.304(3)	4.887(2)	193.25(7)	Pv
	2.887(1)	9.159(3)	7.179(3)	189.81(12)	pPv
16.6	5.397(2)	7.283(2)	4.880(2)	191.82(4)	Pv
	2.881(1)	9.096(2)	7.177(1)	188.04(3)	pPv
20.1	5.345(3)	7.241(3)	4.842(2)	187.38(7)	Pv
	2.866(1)	9.000(3)	7.152(2)	184.49(5)	pPv
14.7	5.405(4)	7.313(6)	4.955(4)	195.86(13)	Pv
	2.898(1)	9.252(2)	7.188(1)	192.73(4)	pPv
9.4	5.426(2)	7.429(3)	5.110(2)	205.98(7)	Pv
	2.931(1)	9.483(1)	7.235(1)	201.13(2)	pPv
6.5	5.453(1)	7.512(2)	5.193(1)	212.72(3)	Pv
	2.955(0)	9.641(1)	7.283(0)	207.43(2)	pPv
3.4	5.486(1)	7.591(1)	5.276(1)	219.74(3)	Pv
	2.986(1)	9.800(1)	7.332(1)	214.51(3)	pPv
1.1	5.522(1)	7.666(1)	5.339(1)	226.01(2)	Pv
	3.009(1)	9.964(1)	7.382(1)	221.30(3)	pPv
0.0	5.534(1)	7.702(2)	5.367(1)	228.78(4)	Pv
	3.019(1)	10.043(2)	7.404(1)	224.45(5)	pPv

and postperovskite above 11.0 GPa. The volume change accompanying the transformation was calculated to be approximately 2% at 12 GPa. The $P-V$ data are plotted in Figure 3. The transition pressure is much lower than 30 GPa for $NaMgF_3$ and is comparable to 18 GPa for $NaZnF_3$. The transformation was not completed even upon further compression to 20 GPa. The diffraction profiles in the decompression process, where hydrostaticity was restored, clearly indicate that some amount of perovskite (approximately 50%) remained untransformed. The bulk moduli (K_0) of the perovskite and postperovskite phases were calculated to be 63.8 ± 2.1 GPa and 65.8 ± 1.7 GPa, respectively, by fitting the third-order Birch–Murnaghan equation of state to the $P-V$ data of the quasihydrostatic compression experiment with a fixed value of K_0' = 4. The bulk moduli of the perovskite and postperovskite phases are significantly lower than those of oxide perovskites and postperovskites,[17−20] as shown in Table 2.

Shirako et al.[13] determined the phase equilibrium line of the perovskite-to-postperovskite transition as P (GPa) = 0.014T (K) − 2, judging from products recovered from high $P-T$ experiments using a multianvil high-pressure apparatus. Considering that the previous study successfully obtained a single phase of postperovskite at 16 GPa and 1273 K, the present sluggish transformation at room temperature could be

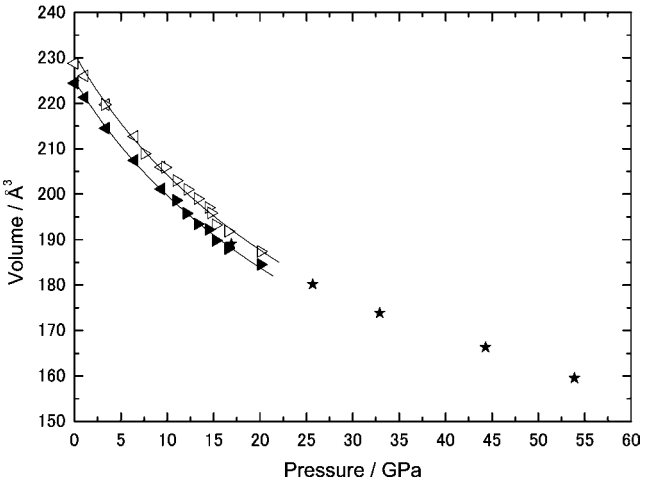

Figure 3. $P-V$ data of $NaNiF_3$ polymorphs. Open triangles (perovskite) and solid triangles (postperovskite) represent the room-temperature compression experimental data. Right- and left-pointing triangles are data from the compression and decompression experiments. Stars (postperovskite) represent data of the laser-heating experiments. Solid lines are the results obtained by fitting the Birch–Murnaghan equation of state to the experimental data under the quasihydrostatic condition.

Table 2. Equation-of-State Parameters (K_0 and K_0') and Cell Volumes (V_0)

compound	phase	V_0 (Å^3)	K_0 (GPa)	K_0'	ref
$NaNiF_3$	Pv	228.33			14
		230.90(85)	63.8(2.1)	4[a]	present work[b]
	pPv	225.07(64)	65.8(1.7)	4[a]	present work[b]
$NaCoF_3$	Pv	236.69			14
		237.81(58)	65.4(1.5)	4[a]	present work[b]
	pPv	231.70(74)	64.4(1.8)	4[a]	present work[b]
$NaZnF_3$	Pv	234.32			14
		236.31(1.28)	64.98(2.67)	4[a]	11
	pPv	229.23(1.53)	69.88(3.69)	4[a]	11
$NaMgF_3$	Pv	224.56			14
		225.13	75.6	4[a]	9
	pPv	200(3)	137(18)	4[a]	9
$MgSiO_3$	Pv	162.6(2)	253(1)	4[a]	17
	pPv	162.86	237(1)	4[a]	19
$MgGeO_3$	Pv	182.90(3)	216(3)	4[a]	18
	pPv	183.10(8)	192(5)	4[a]	20

[a]A fixed value is used. [b]$P-V$ data obtained by quasihydrostatic compression experiments are used for the fitting.

attributed to there being insufficient temperature to enhance the phase transition. Indeed, the laser-heating experiment done at 16.9 GPa obviously accelerated the transition (Figure 4a) because the temperature approached 2000 K. We repeated the laser-heating experiments while increasing the pressure to see if any further transformation took place in $NaNiF_3$. However, we could not find any new phase up to 54 GPa (Figure 4b). As indicated in Figure 4c, the b axis was anisotropically compressed in the postperovskite structure compared with the a and c axes.

Perovskite-to-Postperovskite Transition and Disproportionation in $NaCoF_3$. The room-temperature compression of $NaCoF_3$ perovskite also resulted in a postperovskite phase at 11.8–14.0 GPa (Figure 5). The conversion ratio from perovskite to postperovskite clearly increased with pressure.

dx.doi.org/10.1021/ic300118d | Inorg. Chem. 2012, 51, 6559–6566

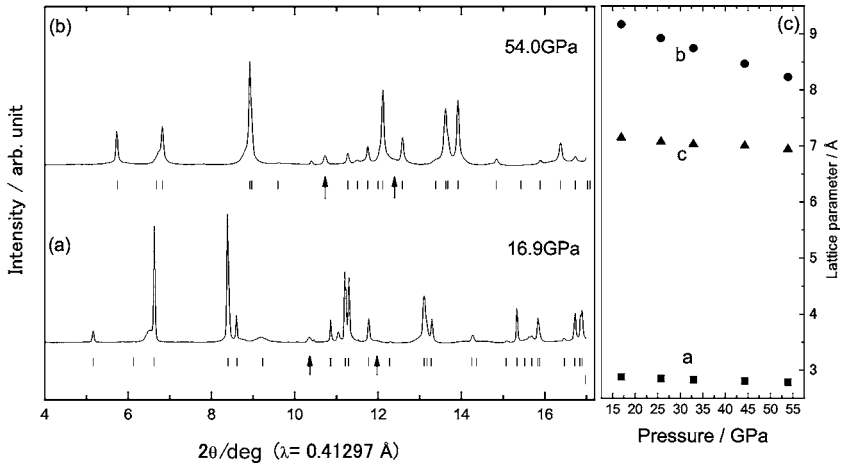

Figure 4. XRD profiles of the laser-heated $NaNiF_3$ sample at 16.9 GPa (a) and 54.0 GPa (b). The profiles are obtained at room temperature after heating. The background was subtracted. Tick marks represent the calculated positions of the diffraction peaks of the postperovskite. Arrows indicate the positions of the diffractions from gold powder. (c) Lattice parameter variation of the laser-heated $NaNiF_3$ postperovskite with pressure.

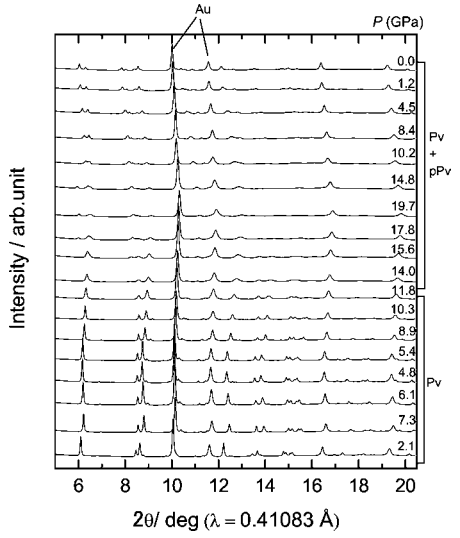

Figure 5. XRD profiles from the $NaCoF_3$ sample under room-temperature compression using a quasihydrostatic pressure medium. Pv and pPv denote the perovskite and postperovskite phases in the diffraction profile. The pressure changes from bottom to top. Au indicates the diffraction peaks from gold powder.

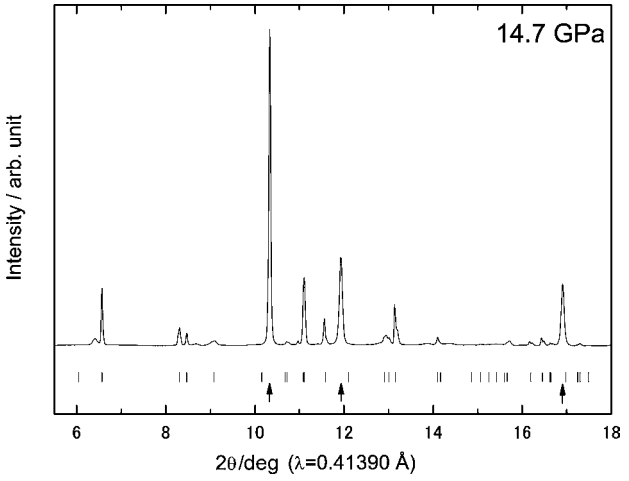

Figure 6. XRD profile from the laser-heated $NaCoF_3$ sample. Tick marks represent the postperovskite phase. Arrows indicate the positions of the diffractions from gold powder.

However, because of the sluggish transformation at room temperature, some of the perovskite phase remained untransformed in the sample recovered from 36 GPa. On the other hand, the postperovskite phase clearly appeared in the laser-heating experiments that were conducted at 14.7−19.3 GPa (Figure 6). The $P-V$ data are plotted in Figure 7 and listed in Table 3. We expected that the laser-heating experiments performed at 31.5 GPa would produce a single postperovskite phase. However, we found neither a postperovskite phase nor a perovskite phase in the SXRD profile. A new pattern clearly appeared in the diffraction profile (Figure 8b). Moreover, after decompression to 1 atm, the SXRD profile exhibited an amorphous-like pattern (Figure 8c). We confirmed that this kind of transition was reproducible in several runs done at 23−28 GPa, of which one of the experiments was performed without any pressure marker.

Note that, before we began the in situ SXRD experiment on $NaCoF_3$, we already had recognized an amorphous-like phase in samples recovered from high-pressure and high-temperature experiments using the multianvil high-pressure apparatus. At that time, we guessed that the amorphous-like phase resulted from the metastability of the postperovskite phase because it is known that several high-pressure postperovskite phases, such as in $MgSiO_3$,[1] $MgGeO_3$,[2] $MnGeO_3$,[3] and Ga_2O_3,[21] likely change into amorphous phases during decompression. Because we confirmed, here, that the $NaCoF_3$ postperovskite phase is quenchable, the unquenchable phase must not be postperovskite but rather a new phase or phases.

We initially supposed the new phase to be a single so-called postpostperovskite phase because neither NaF (NaCl-type structure) nor CoF_2 (rutile-type structure)[22] was found in the XRD patterns of the recovered sample. To find a unit cell, the d values were tested with the indexing program of McMaille.[23] There were no indexing results for cubic, tetragonal, and hexagonal cells. An orthorhombic unit cell and several candidates for monoclinic cells also did not yield a reasonable unit cell volume. Therefore, we tried to examine the composition of the recovered sample synthesized at 23.4 GPa and 1273 K in the multianvil high-pressure apparatus. The scanning electron microscopy back-scattering electron image in

dx.doi.org/10.1021/ic300118d | Inorg. Chem. 2012, 51, 6559−6566

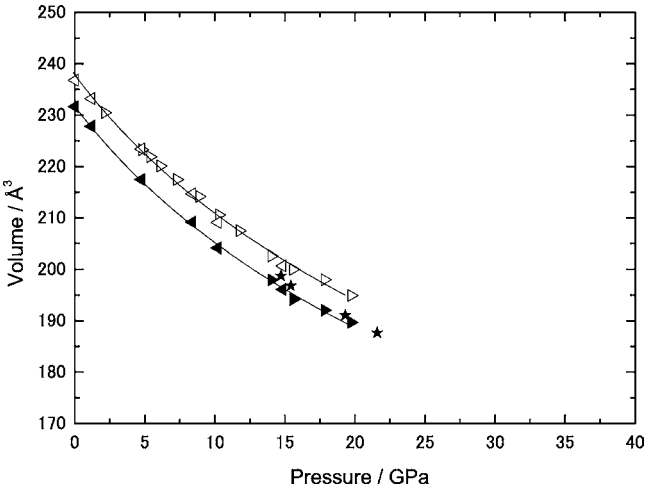

Figure 7. $P-V$ data of $NaCoF_3$ polymorphs. Open triangles (perovskite) and solid triangles (postperovskite) represent the room-temperature compression experimental data. Right- and left-pointing triangles are data from the compression and decompression experiments, respectively. Stars (postperovskite) represent data of the laser-heating experiments. Solid lines are the results obtained by fitting the Birch–Murnaghan equation of state to the experimental data under the quasihydrostatic condition.

Table 3. Unit Cell Parameters and Cell Volumes of $NaCoF_3$ Perovskites (Pv) and Postperovskites (pPv) under Quasihydrostatic Compression

P (GPa)	a (Å)	b (Å)	c (Å)	V (Å^3)	phase
2.1	5.569(0)	7.720(1)	5.360(1)	230.44(2)	Pv
7.3	5.507(0)	7.563(1)	5.221(1)	217.43(2)	Pv
6.1	5.517(0)	7.596(1)	5.252(1)	220.09(2)	Pv
4.8	5.533(0)	7.633(1)	5.287(1)	223.26(2)	Pv
5.4	5.526(0)	7.617(1)	5.271(1)	221.88(2)	Pv
8.9	5.492(0)	7.523(1)	5.182(1)	214.14(2)	Pv
10.3	5.482(1)	7.483(1)	5.132(1)	210.54(2)	Pv
11.8	5.488(1)	7.449(2)	5.076(2)	207.49(4)	Pv
14.0	5.458(3)	7.409(5)	5.010(5)	202.62(11)	Pv
	2.924(5)	9.299(27)	7.302(19)	197.94(50)	pPv
15.6	5.444(5)	7.379(7)	4.980(7)	200.04(14)	Pv
	2.901(3)	9.197(14)	7.275(9)	194.12(25)	pPv
17.8	5.402(2)	7.391(3)	4.959(2)	198.00(7)	Pv
	2.879(1)	9.376(6)	7.115(4)	192.03(9)	pPv
19.7	5.396(13)	7.328(14)	4.930(8)	194.94(33)	Pv
	2.884(3)	9.190(12)	7.157(8)	189.68(22)	pPv
14.8	5.429(3)	7.413(5)	4.987(3)	200.70(13)	Pv
	2.881(2)	9.460(7)	7.144(3)	194.73(14)	pPv
10.2	5.483(3)	7.477(7)	5.100(6)	209.06(13)	Pv
	2.961(1)	9.459(5)	7.288(2)	204.11(8)	pPv
8.4	5.494(2)	7.532(4)	5.187(3)	214.63(9)	Pv
	2.975(1)	9.627(4)	7.304(2)	209.14(7)	pPv
6.5	5.453(1)	7.512(2)	5.193(1)	212.72(3)	Pv
	2.955(0)	9.641(1)	7.283(0)	207.43(2)	pPv
4.7	5.539(2)	7.635(4)	5.282(3)	223.38(10)	Pv
	3.011(1)	9.809(4)	7.364(2)	217.45(9)	pPv
1.2	5.591(2)	7.752(4)	5.381(3)	233.22(8)	Pv
	3.047(2)	10.052(5)	7.439(3)	227.81(14)	pPv
0.0	5.612(1)	7.794(2)	5.414(2)	236.79(5)	Pv
	3.064(1)	10.123(4)	7.468(2)	231.64(9)	pPv

Figure 9 clearly suggests that the recovered sample consists of two phases. Elemental analysis using an electron probe microanalyzer was performed to determine the chemical composition. The analysis resulted in the following disproportionation reaction scheme: $6NaCoF_3 \Rightarrow Na_5Co_3F_{11} + NaCo_3F_7$. So far, unfortunately, we have not been able to discern any structure models from the diffraction profile consisting of the two unknown high-pressure phases.

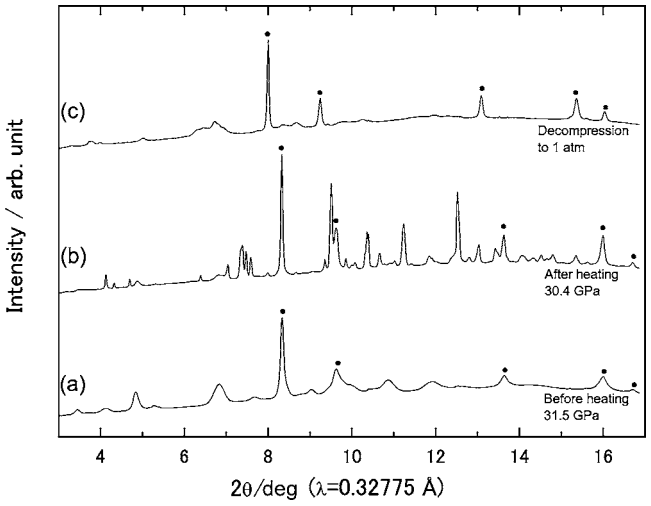

Figure 8. XRD profiles from the $NaCoF_3$ sample: (a) after compression to 31.5 GPa; (b) at 30.0 GPa after heating at about 1500 K; (c) after recovery at ambient pressure. Peaks marked with dots indicate diffractions from gold powder.

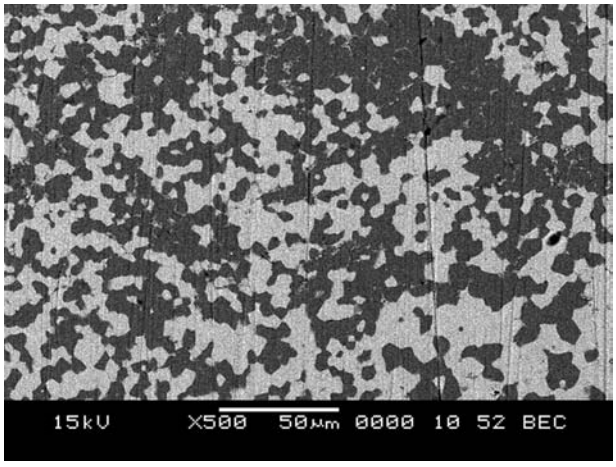

Figure 9. Back-scattering electron image of the recovered sample synthesized at 23.4 GPa and 1273 K using the multianvil high-pressure apparatus. Bright and dark areas exhibit the composition difference between the sodium- and cobalt-rich phases, respectively.

We conducted sample recovery experiments using the multianvil high-pressure apparatus to ascertain the exact $P-T$ boundary of the disproportionation reaction (Table 4). The phase diagram is depicted in Figure 10. The perovskite–postperovskite boundary with a positive slope shows the same trend as that reported for $NaNiF_3$. On the other hand, a negative slope is proposed for the postperovskite–disproportionation product boundary in $NaCoF_3$.

Compressible Behavior Relevant to Perovskite-to-Postperovskite Transformation in $NaB^{2+}F_3$ (B = Ni, Co, Zn, Mg). We know the compression behaviors of $NaCoF_3$ and $NaNiF_3$ perovskites in addition to those of $NaZnF_3$ and $NaMgF_3$ perovskites, so it is worth considering the systematics

dx.doi.org/10.1021/ic300118d | Inorg. Chem. 2012, 51, 6559–6566

Table 4. Results of the High-Pressure and High-Temperature Experiments in $NaCoF_3$

run no.	P (GPa)	T (K)	time (min)	phase
18	14	1173	30	Pv
19	14.5	1173	30	pPv
17	15	1173	30	pPv
15	15.5	1173	30	pPv
13	16	1173	30	pPv
11	19	1173	30	pPv
12	19.5	1173	30	pPv
14	20	1173	30	dispro.[a] + pPv
21	20.5	1173	30	dispro.
2	15	1273	30	Pv
4	16	1273	30	Pv
16	16.5	1273	30	pPv
8	17	1273	30	pPv
24	18	1273	10	pPv
22	18.5	1273	30	dispro. + pPv
7	19	1273	30	dispro. + pPv
23	19.5	1273	30	dispro.
6	20	1273	30	dispro.
1	23.4	1273	30	dispro.
28	17	1373	30	Pv
26	17.5	1373	30	Pv + pPv[b]
20	18	1373	30	dispro. + pPv
27	18.5	1373	30	dispro.
3	23.4	1373	30	dispro.
10	18	1473	30	Pv
25	18.5	1473	30	dispro. + Pv
9	19	1473	30	dispro.
5	23.4	1473	30	dispro.

[a]Disproportionation phases. [b]The run product is almost Pv and a small amount of pPv.

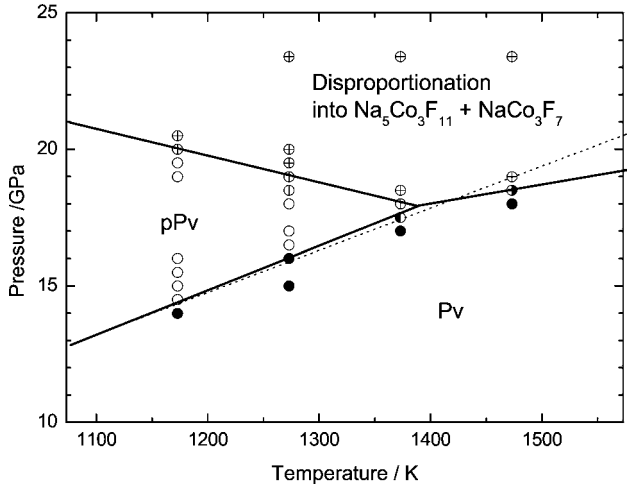

Figure 10. Phase diagram of $NaCoF_3$ plotted on the basis of data from recovery experiments using the multianvil high-pressure apparatus. Solid circles, open circles, circles with crosses, circles with bars, and half solid circles indicate perovskites, postperovskites, disproportionation phases, mixtures of postperovskite and disproportionation phases, and mixtures of perovskite and disproportionation phases, respectively. The dotted line indicates the phase boundary of perovskite–postperovskite in $NaNiF_3$.[13]

of the perovskite-to-postperovskite phase transformations in $NaB^{2+}F_3$. It was suggested that the transition to the $CaIrO_3$-type postperovskite structure can be explained by the extrapolated compressive behavior of the $GdFeO_3$-type orthorhombic perovskite.[4,24] Ab initio calculations by Tsuchiya et al. indicated that the shear strain ε_6 enhances the perovskite-to-postperovskite transformation.[24] This transition mechanism would be involved in tilting the BO_6 octahedron. Tateno et al.[4] listed the tilt angles (Φ)[25] of various oxide perovskites that could transform into the postperovskite structure. They concluded that if Φ is greater than 15° and that if it increases with increasing pressure, the perovskite phase would eventually change into the postperovskite phase. Moreover, they suggested that the transition mostly occurs at $\Phi \sim 25°$. We plotted the tilt angle $\Phi = \cos^{-1}(\sqrt{2}c^2/ab)$ of the present $NaB^{2+}F_3$ perovskites with pressure on the assumption of rigid regular octahedra for BF_6 (Figure 11). In the plot, we can clearly see that both

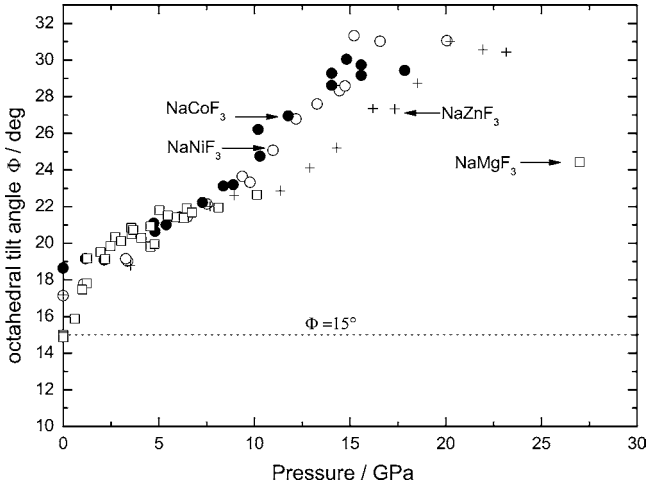

Figure 11. Octahedral tilt angle (Φ) of various fluoroperovskites. Solid circles ($NaNiF_3$) and open circles ($NaCoF_3$) were calculated from the lattice parameters determined in this study. Crosses ($NaZnF_3$) and open squares ($NaMgF_3$) were calculated from data in the literature.[9,11,26] Arrows indicate the perovskite-to-postperovskite transition pressure of each compound.

$NaCoF_3$ and $NaNiF_3$ exhibit Φ greater than 15° over the whole pressure range and that Φ has an upward trend with increasing pressure. Furthermore, perovskite-to-postperovskite transitions take place at $\Phi = 26–27°$, which is consistent with the $\Phi \sim 25°$ suggested by Tateno et al.[4] The tilt angles of $NaZnF_3$ and $NaMgF_3$, as calculated from the literature,[10,11,26] also have the same trend as our data (Figure 11), except for rather high transition pressures of ~18 and ~26 GPa, respectively.

The tolerance factor, $t = (r_A + r_X)/\sqrt{2}(r_B + r_X)$,[27] where r denotes the effective ionic radii[28] of each element in ABX_3 compounds, is a useful indicator for discussing deviations from the ideal perovskite. In the $GdFeO_3$ type of orthorhombic perovskites, t decreases as the tilt angle of the BX_6 octahedra increases. To discuss how t behaves under high pressure, we should note the electronegativity of B, which governs the B–F bonding properties. The Pauling electronegativities[29] of Mg, Zn, Co, and Ni lead to corresponding values of 1.31, 1.65, 1.88, and 1.91, respectively. The Mg–F bond has the highest ionicity among them, so it would have relatively weak and compressible properties compared with the other B–F bonds. This bond property makes the value of t rather insensitive to pressure. Therefore, relatively higher pressure was needed for the $NaMgF_3$ perovskite to tilt the BF_6 octahedra to the transition point. Thus, the perovskite-to-postperovskite transitions in

dx.doi.org/10.1021/ic300118d | Inorg. Chem. 2012, 51, 6559–6566

fluoroperovskites are like those in oxide perovskites in that they strongly depend on the tilt angle of the octahedra. On the other hand, the transition pressures of these fluoroperovskites are much lower than those of oxide perovskites (e.g., 120 GPa for $MgSiO_3$, 68 GPa for $MgGeO_3$, and 60 GPa for $MnGeO_3$).[1−3] Moreover, sodium fluoroperovskites easily transform into postperovskites at room temperature, in contrast to the crystallization of oxide postperovskites requiring high temperature. This difference might be attributed to the compressible behavior of sodium fluoroperovskites. As mentioned above, the bulk moduli of fluoroperovskites (Table 2) are significantly lower than those of oxide perovskites (e.g., K_0 = 253 GPa for $MgSiO_3$ and K_0 = 216 GPa for $MgGeO_3$).[17,18] We should also note the difference in linear compressibility between oxide and sodium fluoroperovskites. As shown in Table 5, the linear compressibilities of the *a*, *b*, and *c* axes of $MgSiO_3$ and $MgGeO_3$ perovskites are (0.9−1.1) × 10^{-3} GPa^{-1}, (1.4−1.6) × 10^{-3} GPa^{-1}, and (1.4−2.2) × 10^{-3} GPa^{-1}, respectively. In contrast, those of fluoroperovskites are higher: β_a = (1.7−2.7) × 10^{-3} GPa^{-1}, β_b = (4.6−4.8) × 10^{-3} GPa^{-1}, and β_c = (6.9−9.0) × 10^{-3} GPa^{-1}. These high values reflect the low bulk modulus of fluoroperovskites. More noticeable is anisotropic compression in sodium fluoroperovskites. In both oxide and fluoroperovskites, β_c gives the highest axial compressibility. In particular, β_c is more than 3 times β_a in sodium fluoroperovskites. Because the octahedral tilt angle is derived from $\cos^{-1}(\sqrt{2c^2/ab})$, significant compression on the *c* axis affects the degree of tilt more than compression on the *a* or *b* axis. Thus, the tilt of the BF_6 octahedron is very sensitive to pressure. Consequently, this kind of anisotropic compressible behavior in sodium fluoroperovskites ends up lowering the transition pressure and may enable transitions even at room temperature. The reason why octahedra in sodium fluoroperovskites can be so heavily tilted can also be investigated from the viewpoint of electron negativity. At ambient pressure, there are no large differences between the tolerance factors of oxide perovskites (e.g., $MgGeO_3$ and $MgGeO_3$; *t* = 0.84−0.89) and fluoroperovskites (e.g., $NaCoF_3$ and $NaNiF_3$; *t* = 0.86−0.88). On the other hand, the bond ionicity, which can be estimated from the electronegativities,[29] of Na−F is much higher than that of Mg−O. This means that the Na−F bond, which is much weaker than the Mg−O bond, likely enhances the orthorhombic distortion in the perovskite structure as the pressure increases, and the tolerance factor would be significantly reduced. As a result, the octahedra of fluoroperovskites would be heavily tilted.

Table 5. Comparison of Linear Compressibilities (β) between Oxide and Sodium Fluoroperovskites

compound	$\beta_a \times 10^{-3}$ (GPa^{-1})	$\beta_b \times 10^{-3}$ (GPa^{-1})	$\beta_c \times 10^{-3}$ (GPa^{-1})	ref
$NaNiF_3$	2.0(1)	4.7(1)	9.0(4)	present work
$NaCoF_3$	2.6(1)	4.8(2)	8.3(3)	present work
$NaZnF_3$	1.7(1)	4.6(1)	7.8(2)	11
$NaMgF_3$	2.7	4.8	6.9	26
$MgSiO_3$	1.1	1.4	1.4	18
$MgGeO_3$	0.9	1.6	2.2	18, 30

Perspective on Postpostperovskite Phase Transtions in $NaB^{2+}F_3$. We anticipated that a postpostperovskite phase would appear in our experiments. However, instead of a postpostperovskite phase, we found a disproportionation reaction in $NaCoF_3$. Certain reports have mentioned postpostperovskite phases in $NaB^{2+}F_3$. Martin et al. reported a postpostperovskite phase (N phase) in a laser-heated sample of $NaMgF_3$ at 37−55 GPa.[9] On the other hand, a recent laser-heating experiment by Grocholski et al. could not reproduce the N phase in $NaMgF_3$ and instead found a stable postperovskite phase up to 74 GPa.[12] Despite the lack of laser-heating experiments on $NaZnF_3$, Yakovlev et al. mentioned that an additional X-ray peak appeared on the XRD profile of the $NaZnF_3$ postperovskite above 25 GPa at room temperature.[11] However, in their report, all of the other peaks were assigned to a $CaIrO_3$-type structure for pressures up to 40 GPa. Thus, we are unable at present to conclude that the additional peak is due to a stable structure. Therefore, the existence of the postpostperovskite phase in $NaB^{2+}F_3$ remains an open question.

It is worth noting that postperovskite disproportionation was only found in $NaCoF_3$. Among B^{2+} mentioned above, only Co^{2+} could have spin crossover. It is known that changes in the spin state affect the structural transition (e.g., Oka et al.[30]). Therefore, it is possible that spin crossover may be the cause of the disproportionation reaction in $NaCoF_3$. Accordingly, high-pressure X-ray emission spectroscopy measurements on Co^{2+} should be done to clarify this point.

SUMMARY

We confirmed the existence of perovskite-to-postperovskite phase transitions in $NaNiF_3$ and $NaCoF_3$ by using the in situ XRD method under high pressure. Unlike oxide perovskites, sodium fluoroperovskites easily transform into the postperovskite structure even at room temperature. Anisotropic compression behavior mainly derived from the linear compressibility along the *c* axis (β_c) causes the BF_6 octahedral tilt to increase rapidly, which triggers a transformation into the postperovskite phase. The $NaCoF_3$ postperovskite broke down into two unquenchable phases after laser heating above 25 GPa. This kind of disproportionation never occurs in $NaNiF_3$ and did not correspond to the reported postpostperovskite transformation in $NaMgF_3$. The emergence of the disproportionation might be attributed to a spin-state change potentially present in Co^{2+} because no spin-state change exists in Ni^{2+}.

AUTHOR INFORMATION

Corresponding Author

*E-mail: yusa.hitoshi@nims.go.jp.

Notes

The authors declare no competing financial interest.

ACKNOWLEDGMENTS

The SXRD experiments were conducted at BL-10XU and BL04B2 in SPring-8 and AR-NE1 in KEK-PF with the approval of JASRI (Proposal Nos. 2011A1171, 2010A1185, and 2011A1171) and KEK (Proposal Nos. 2009G052 and 2011G545), respectively. H.Y. and M.A. acknowledge support from Grants-in-Aid for Scientific Research from JSPS (Grant 22340164 to H.Y. and Grant 22340163 to M.A.). We thank K. Kosuda for his help with electron probe microanalysis.

REFERENCES

(1) Murakami, M.; Hirose, K.; Kuwayama, K.; Sata, N.; Ohishi, Y. *Science* **2004**, *304*, 855.

(2) Hirose, K.; Kuwayama, K.; Ohishi, Y.; Tateno, S.; Sata, N. *Am. Mineral.* **2005**, *90*, 262.
(3) Tateno, S.; Hirose, K.; Sata, N.; Ohishi, Y. *Phys. Chem. Miner.* **2006**, *32*, 721.
(4) Tateno, S.; Hirose, K.; Sata, N.; Ohishi, Y. *Phys. Earth Planet. Inter.* **2010**, *181*, 54.
(5) Okada, T.; Yagi, T.; Nishio-Hamane, D. *Phys. Chem. Miner.* **2011**, *38*, 251.
(6) Nishio-Hamane, D.; Yagi, T.; Ohshiro, M.; Niwa, K.; Okada, T.; Seto, Y. *Phys. Rev. B* **2010**, *82*, 092103.
(7) Wu, X.; Steinle-Neuman, G.; Narygina, O.; Kantor, I.; McCammon, C.; Prakapenka, V.; Swamy, V.; Dubrovinsky, L. S. *Phys. Rev. Lett.* **2009**, *103*, 065503.
(8) Fernando, A.; Fernando, R.; Hirai, S.; Walsh, J. N.; Lennie, A.; Redfern, S. A. T. *High Pressure Res.* **2008**, *28*, 539.
(9) Martin, C. D.; Crichton, W. A.; Liu, H.; Prakapenka, V.; Chen, J.; Parise, J. B. *Geophys. Res. Lett.* **2006**, *33*, L11305.
(10) Martin, C. D.; Crichton, W.; Liu, H.; Prakapenka, V. B.; Chen, J.; Parise, J. B. *Am. Mineral.* **2006**, *91*, 1703.
(11) Yakovlev, S.; Avdeev, M.; Mohamed, M. *J. Solid State Chem.* **2009**, *182*, 1545.
(12) Grocholski, B.; Shim, S. H.; Prakapenka, V. B. *Geophys. Res. Lett.* **2010**, *37*, L14204.
(13) Shirako, Y.; Shi, Y. G.; Aimi, A.; Mori, D.; Kojitani, H.; Yamaura, K.; Inaguma, Y.; Akaogi, M. *J. Solid State Chem.* **2012**, in press, http://dx.doi.org/10.1016/j.jssc.2012.03.004.
(14) Lütgert, B.; Babel, D. *Z. Anorg. Allg. Chem.* **1992**, *616*, 133.
(15) Hammersley, A. P. European Synchrotron Radiation Facility Internal Report ESRF97HA02T, 1997
(16) Larson, A. C.; Dreele, R. B. V. *Los Alamos Natl. Lab. (Rep.)* **2004**, 86−748.
(17) Vanpeteghem, C. B.; Zhao, J.; Angel, R. J.; Ross, N. L. *Geophys. Res. Lett.* **2006**, *33*, L03306.
(18) Runge, C. E.; Kubo, A.; Kiefer, B.; Meng, Y.; Prakapenka, V. B.; Shen, G.; Cava, R. J.; Duffy, T. S. *Phys. Chem. Miner.* **2006**, *33*, 699.
(19) Ono, S.; Kikegawa, T.; Ohishi, Y. *Am. Mineral.* **2006**, *91*, 475.
(20) Hirose, K.; Kawamura, K.; Ohishi, Y.; Tateno, S.; Sata, N. *Am. Mineral.* **2005**, *90*, 262.
(21) Tsuchiya, T.; Yusa, H.; Tsuchiya, J. *Phys. Rev. B* **2007**, *76*, 174108.
(22) According to our preliminary laser-heating experiments for CoF_2, a PdF_2-type structure under high pressure reverts to a rutile structure at ambient condition. The details will be described elsewhere.
(23) LeBail, A. *Powder Diffr.* **2004**, *19*, 249.
(24) Tsuchiya, T.; Tsuchiya, J.; Umemoto, K.; Wentzcovitch, R. M. *Earth Planet. Sci. Lett.* **2004**, *224*, 241.
(25) O'Keeffe, M.; Hyde, B. G.; Bovin, J. O. *Phys. Chem. Miner.* **1979**, *4*, 299.
(26) Zhao, Y.; Weidner, D. J.; Ko, J.; Leinenweber, K.; Liu, X.; Li, B.; Meng, Y.; Pacalo, R. E. G.; Vaughan, M. T.; Wang, Y.; Yeganeh-Haeri, A. *J. Geophys. Res.* **1994**, *99*, 2871.
(27) Goldschmidt, V. M. *Naturwissenschaften* **1926**, *14*, 477.
(28) Shannon, R. D. *Acta Crystallogr., Sect. A* **1976**, *32*, 751.
(29) Pauling, L. *The Nature of the Chemical Bond*; Cornell University Press: Ithaca, NY, 1960; p 93.
(30) Oka, K.; Azuma, M.; Chen, W.; Yusa, H.; Belik, A.; Takayama-Muromachi, E.; Mizumaki, M.; Ishimatsu, N.; Hiraoka, N.; Tsujimoto, M.; Tucker, M. G.; Attfield, J. P.; Shimakawa, Y. *J. Am. Chem. Soc.* **2010**, *132*, 9438.